Thickness-Dependent Coloration Properties of Glass-Substrate Viologen-Based Electrochromic Devices

David Barrios,[1] **Ricardo Vergaz,**[1] **Juan Carlos Torres-Zafra,**[1] **César Vega,**[1] **José Manuel Sánchez-Pena,**[1] ***Senior Member, IEEE*, and Ana Viñuales**[2]

[1]Grupo de Displays y Aplicaciones Fotónicas, Departamento Tecnología Electrónica, Universidad Carlos III de Madrid, E28911, Leganés, Spain
[2]Center for Electrochemical Technologies (CIDETEC), Departamento Nuevos Materiales, Parque Tecnológico de San Sebastián, E-20009, San Sebastián, Spain

DOI: 10.1109/JPHOT.2012.2227249
1943-0655/$31.00 ©2012 IEEE

Manuscript received October 19, 2012; accepted October 28, 2012. Date of current version November 15, 2012. This work was supported by the Comunidad Autónoma de Madrid under Grant S2009/ESP-1781, FACTOTEM-2. Corresponding author: R. Vergaz (e-mail: rvergaz@ing.uc3m.es).

Abstract: Blue viologen-based electrochromic devices on glass substrates were constructed with different internal active layer thickness by means of a thermoplastic spacer (DuPontTM surlyn1702). Optical measurements, chronoamperometry, and cyclic voltammetry (CV) were the techniques used for characterization. Coloration properties such as switching times for coloring and bleaching processes, coloration efficiency, and effective charge density, previously studied for a single device, are now obtained for several devices with different thicknesses. Dependence on thickness in the response times and in voltage-dependent parameters of device equivalent electric circuit model was studied in previous works. In this paper, some of those parameters, such as Warburg diffusion, double-layer capacitance, and charge transfer resistance, obtained with electrochemical impedance spectroscopy, are related with the coloration properties and their dependence on the thickness obtained by the aforementioned chronoamperometric and CV characterization.

Index Terms: Electrochromics, viologens, electrooptical devices, optical properties, impedance spectroscopy, cyclic voltammetry (CV).

1. Introduction

Electrochromic (EC) materials and devices change their color in response to an external electrical potential. Viologens are organic type-I soluble EC materials (1,1′-disubstituent-4,4′-bipyridilium) showing a feeble or colorless appearance in the dicationic form and colored, after one electron reduction, in the radical cation form, color of which depends on the substituents R and R′. If they interact with the bipyridine core, a reddish black color is obtained if $R = R' =$ phenyl, and an olive green is obtained if the two substituents are p-cyanophenyl. The radical cation is blue in all cases where the substituents $R = R'$ are not in conjugation with the bipyridine core, which is the case for $R = R' =$ alkyl [1]. Short alkyl chains are blue or bluish purple color, due to shift in the absorption band of the spectrum from blue to red depending on their concentration and temperature [2], [3], because of the red color of the dimer, and changing to crimson color as alkyl chains length increases. Viologens are one of the active components within the only mass-produced EC device presently available, the automatically self-darkening car rear-view mirrors developed by Gentex Corporation [4], being also good candidates for EC displays and RGB cells applications [5]–[7]. As

type I, a small continuous electrical current is required for the device coloration maintenance to replenish the colored electrochromes lost by the mutual redox reaction in solution.

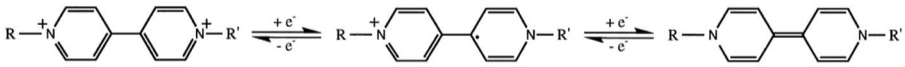

In this paper, five EC devices were manufactured using a viologen material for a room-temperature mixture [8] deposited over ITO glass controlling the internal layer thickness by means of a spacer. This EC mixture is composed of all the electroactive materials (electrolyte, EC, and ion storage material) needed for the EC devices to work and can be applied at room temperature on the transparent conducting substrate (even plastics), leading to a highly transparent device that can switch to blue coloration. Chronoamperometry (ChrA) and chronocoulometry (ChrC), cyclic voltammetry (CV), and electrochemical impedance spectroscopy (EIS) techniques were used for electrochemical characterization. Spectral optical transmittance $T_{spectral}(\%)$ was simultaneously measured with EIS experiments at different dc bias voltage for several coloration levels. Temporal dependence of the transmittance at 600-nm wavelength was simultaneously measured with ChrA and ChrC experiments $(ChrT_{600\,nm})$ and with CV experiments $(CT_{600\,nm})$, respectively.

2. Experimental Details

2.1. Materials

4,4′-Bipyridine (98%) and 1-bromoethane (98%) were purchased by Aldrich and used without further purification. Hydroquinone (99.5%) was obtained from Riedel-de-Haën, and 1-butyl-3-methylimidazolium tetrafluoroborate (99%) was obtained from Solvionic. Extra pure solvents (N,N-dimethylformamide, ethyl acetate, and propylene carbonate) were supplied by Scharlau. Surlyn 1702 (thickness of 50 μm) was purchased by DuPontTM. Amosil 4H and Amosil 4R were obtained from Solaronix. ITO-coated glass slides (glass thickness: 1.1 mm; ITO thickness: 100 nm; $R = 30-50\ \Omega/)$ were a gift of Solems.

2.2. Methods

2.2.1. Synthesis of 1,1′-diethyl-4,4′-bipyridilium Dibromide

The synthesis was carried out according to the procedure reported in [9] with some slight modifications. A mixture of 4,4′-bipyridine (1g, 0.0064 mol) and 1-bromoethane (2.8 g, 0.0256 mol) in 10 mL of DMF was refluxed while stirring for 3 h. The precipitate was filtered off, and the crude product was washed with hot ethyl acetate several times, to yield a yellow solid (2.3 g, 95% yield). 1H NMR (DMSO-d6, 500 MHz): $\delta = 9.48$ (d, 4H, bipyridine, $J = 6.5$ Hz), 8.85 (d, 4H, bipyridine, $J = 6.5$ Hz), 4.77 (m, 4H, N-CH_2), and 1.60 (t, 6H, CH_3, $J = 7.3$ Hz).

2.2.2. Preparation of the EC Mixture and Devices Construction

1,1′-diethyl-4,4′-bipyridilium dibromide (0.01g, 0.027 mmol), hydroquinone (0.003 g, 0.027 mmol), 1-butyl-3-methylimidazolium tetrafluoroborate (1.6 g), and propylene carbonate (2 g) were mixed for 1 h at room temperature. ITO-coated glass slides $(3 \times 2\ cm^2)$ were washed subsequently with water, acetone, and isopropanol and dried with nitrogen stream. ITO/glass cells were prepared by joining two slides through a thermoplastic spacer (Surlyn 1702) placed along the whole perimeter but with an opening (1 mm wide) in one corner. The spacer becomes sticky after heating at 130 °C for a few minutes. In order to prepare devices of different thicknesses, different number of Surlyn layers (from one to five) were applied. Thicknesses of 50, 100, 150, 200, and 250 μm should thus have been obtained. However, according to the measurements made with a micrometer, the real final thicknesses were 60, 90, 130, 180, and 230 μm. The cell was evacuated in a vacuum chamber. Then, it was dipped in the EC mixture and filled through the opening introducing Argon into the vacuum chamber. Once filled with the EC mixture, the edges of the cell were sealed with a mixture of Amosil 4H (45% wt) and Amosil 4R (55% wt), being allowed to cure at room-temperature

Fig. 1. Photograph of EC device of 230 micrometers thickness at 0 V for the colorless state (left) and 2.5 V for the colored state (right).

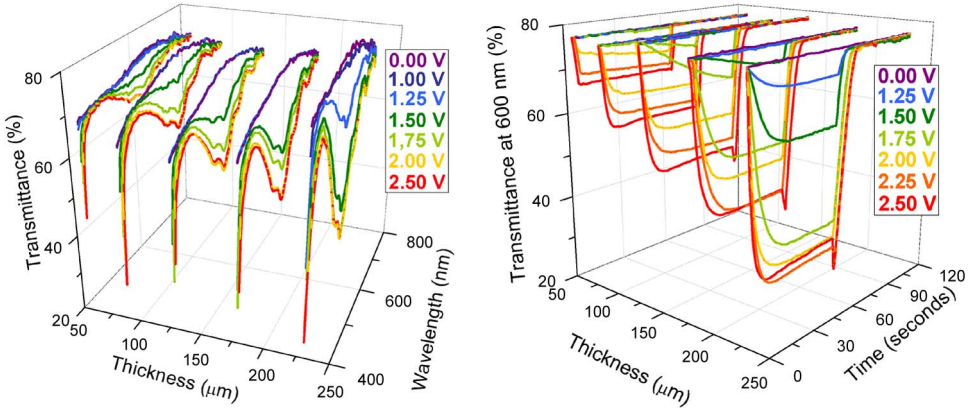

Fig. 2. Thickness dependence spectral $T_{spectral}(\%)$ (left) and time domain $ChrT_{600\,nm}(\%)$ (right) transmittances.

overnight. Fig. 1 shows a photograph of the 230-μm thickness device at colorless and colored states applying 0 and 2.5 V, respectively [10].

2.3. Characterization Setup

Spectral transmittance T was measured using an Ocean Optics USB2000+ spectrometer in the 400- to 800-nm range, a system with up to 1000 spectra per second, a signal-to-noise ratio of 250 : 1, and a full-width half-maximum (FWHM) under 10 nm in the specified wavelength range. ChrA and ChrC, and CV experiments were carried out using FAS2 Gamry potentiostat. $ChrT_{600\,nm}$ and $CT_{600\,nm}$ transmittances were measured by using a spectrometer based on an Acton Research monochromator and a Hamamatsu photomultiplier tube, a system with 5-nm resolution and 1% error in radiance measurements. EIS experiments were carried out using the impedance analyzer Solartron 1260 with frequency ranges from 1 MHz to 10 mHz and 100 mV of ac signal and varying the dc bias voltage signal between 0 and 2.5 V with 0.25-V steps.

3. Results

3.1. Optical Measurements

Fig. 2 (left) shows a 3-D plot of the T dependence with the thickness of the internal layer of the EC devices. The thicker the internal layer, the higher number of color centers formed and, hence, the deeper colored state. Colorless state with 0 V is highly transparent, with values of $T_{600\,nm}$ close to 78%. No variation of T is observed until a threshold dc bias voltage value of 1.5 V is reached (1.25 V for 230 μm), appearing a blue coloration due to an absorption band at wavelengths near the red interval

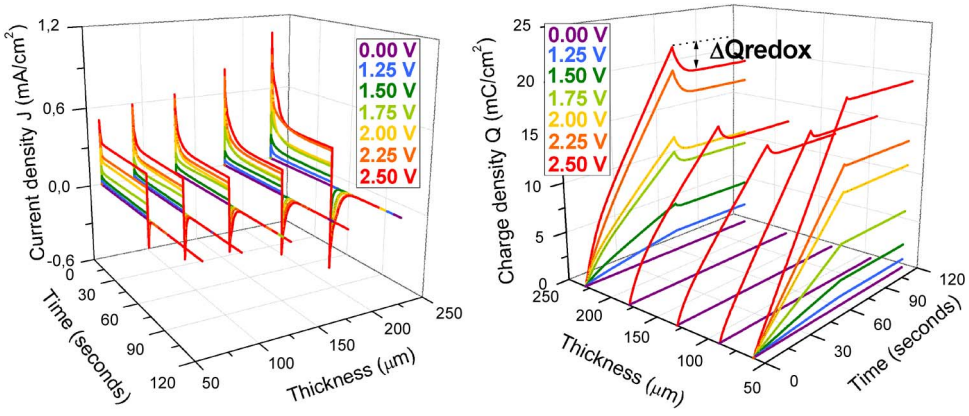

Fig. 3. Thickness dependence current (left) and charge (right) densities J $(\mathrm{mA/cm^2})$ and Q $(\mathrm{mC/cm^2})$ results derived from ChrA and ChrC experiments.

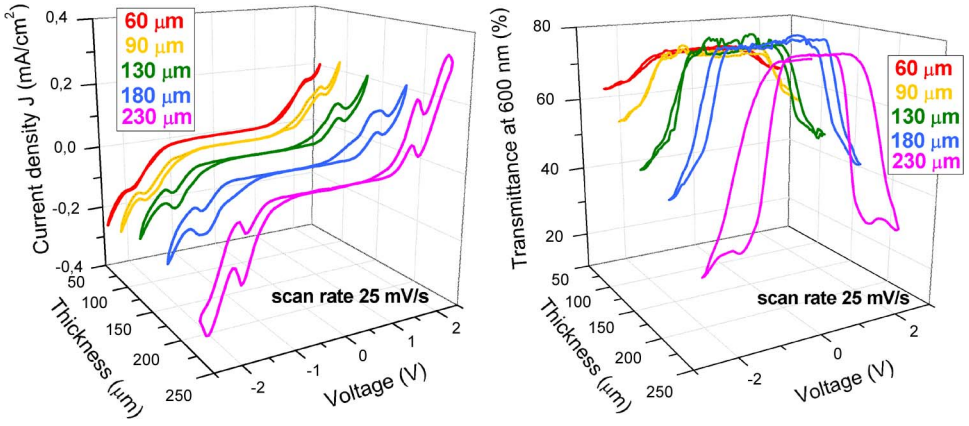

Fig. 4. (Left) Thickness dependence of the current density J $(\mathrm{mA/cm^2})$ and (right) simultaneous cyclic transmittance at 600 nm $\mathrm{CT_{600\,nm}}(\%)$ from the third cycle of CV experiments at 25 mV/s scan rate.

of the optical spectrum. Fig. 2 (right) shows the thickness dependence of the $\mathrm{ChrT_{600\,nm}}$ measured while applying a square voltage signal from V_1 to 0 V with 120 s of period and varying V_1 from 1.25 to 2.5 V with 0.25-V steps. The voltage level for maximum coloration is observed to be 2.50 V for the thinner devices (from 60 to 130 μm). No appreciable changes in T are observed applying potentials higher of 2.25 and 2.00 V to the thicker devices of 180- and 230-μm thicknesses, respectively.

3.2. Electrochemical Measurements From ChrA and ChrC Experiments

Fig. 3 shows the current density J $(\mathrm{mA/cm^2})$ and charge density Q $(\mathrm{mC/cm^2})$ measured from ChrA and ChrC experiments performed simultaneously with the $\mathrm{ChrT_{600\,nm}}$ measurements in Fig. 2 (right). Current and charge density plots show two different behaviors, from 0 to 60 and from 60 to 120 s, related to coloration and bleaching processes, respectively. Further details will be given in the discussion section.

3.3. Electrochemical Measurements From CV Experiments

Fig. 4 shows the thickness dependence of the current density J $(\mathrm{mA/cm^2})$ of CV experiments and the simultaneously measured $\mathrm{CT_{600\,nm}}$. The results are obtained from the third cycle of CV experiments at 25-mV/s scan rate from -2.5 V to $+2.5$ V. A symmetrical redox reaction [see Fig. 4 (left)] is observed due to the symmetry of construction of the solution type-I viologen-based EC devices. As it will be detailed in the discussion section, the area of the voltammogram is related with the coloration contrast observed in the devices [see Fig. 4 (right)]. Slight differences in the

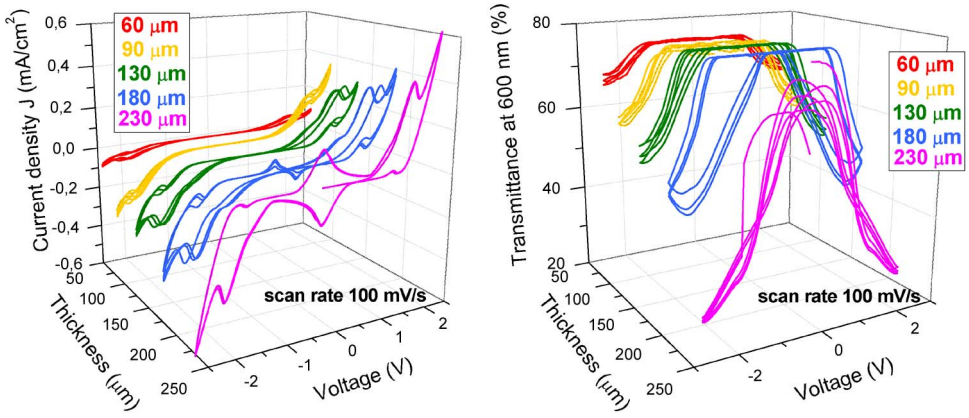

Fig. 5. (Left) Current density J $(\mathrm{mA/cm^2})$ and (right) simultaneous cyclic transmittance at 600 nm $\mathrm{CT_{600\,nm}}(\%)$ from 3 cycles of CV experiments at 100 mV/s scan rate.

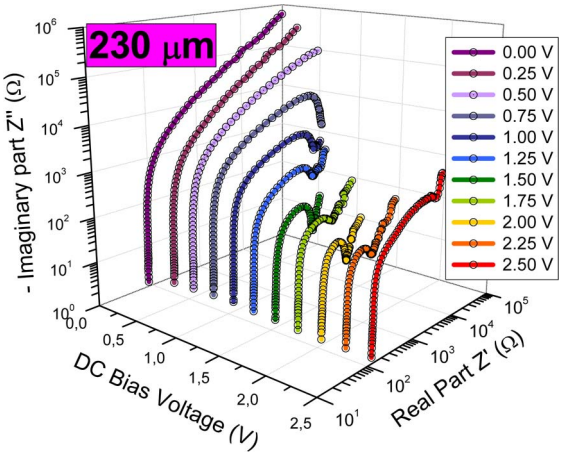

Fig. 6. Nyquist impedance diagrams for different coloration levels for the 230 μm device.

voltammograms of the thicker devices were observed at around $\pm$0.5 V for faster scan rates. In particular, these effects were observed for the device of 230 μm at 50-mV/s scan rate and for the devices of 180 and 230 μm at 100-mV/s scan rate (shown for comparison with the previous figure in Fig. 5). The rate of the reaction seems to be slower than the scan rate as the thickness increases, being not fast enough for the 230-μm thickness device at 100-mV/s scan rate since $\mathrm{CT_{600\,nm}}$ does not completely recover the colorless state [see Fig. 5 (right)].

3.4. Electrochemical Measurements From EIS Experiments

Fig. 6 shows the Nyquist diagrams of the impedance measurement for the 230-μm device (as a representative example of the results in the devices) at the different dc bias voltage levels from 0 to 2.5 V with 0.25-V steps. Logarithmic scales were used for a complete visualization due to the big differences of magnitudes between the colorless and the colored states of the devices. Impedance decrement is observed for the five devices in the coloration process.

4. Discussion

4.1. Optical Measurements

Fig. 7 (left) shows the dependence on thickness for the transmittance contrast at 600 nm $(\Delta \mathrm{T_{600\,nm}})$. Defined as the difference between the maximum (at 0 V applied) and minimum (at 2.5 V)

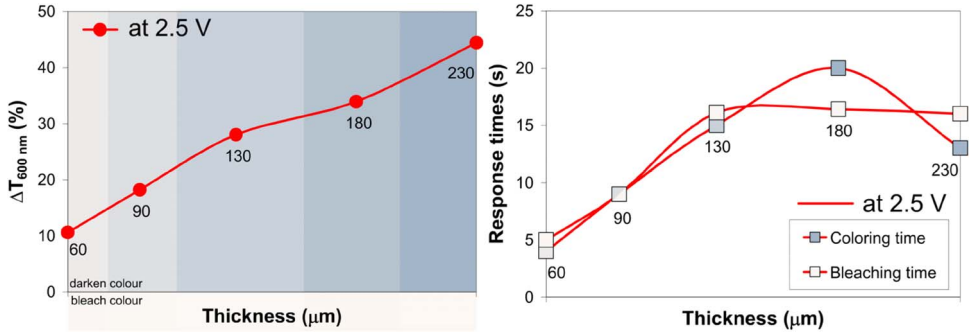

Fig. 7. Thickness dependences: (left) Transmittance contrast at 600 nm ($\Delta T_{600\,nm}$) and simulated background color. (Right) Response times (coloring and bleaching).

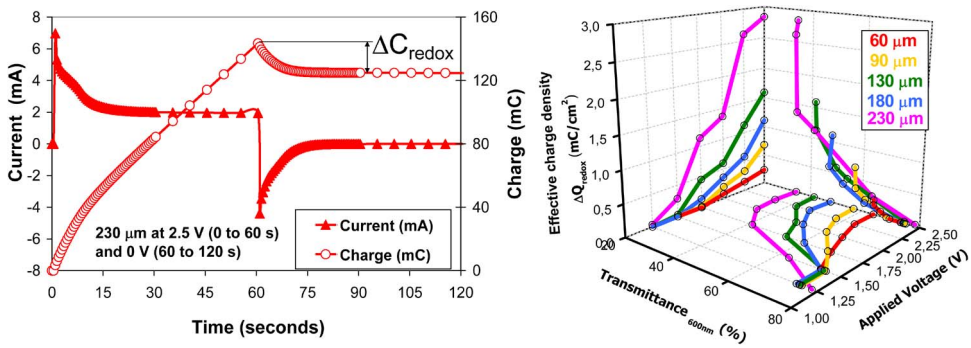

Fig. 8. (Left) Current and charge measurements of ChrA and ChrC experiments at 2.50 V for the 230 μm thickness device. (Right) Thickness dependence effective charge density variation ΔQ_{redox} and optical transmittance of coloration state for applied voltages from 1.00 to 2.50 V. Only projections over the walls are plotted for a better visualization.

optical transmissions, $\Delta T_{600\,nm}$ depends clearly on the thickness of the devices. The background color plotted on the graph is calculated from the spectral transmittance applying the CIE YXY chromaticity and luminance coordinates, and the XYZ to sRGB color space conversion matrix. It simulates the color appearance of the five devices when colored at 2.5 V. The thickness dependence of the response times, calculated as the time to change from a 10 to a 90% of the contrast, is shown in Fig. 7 (right). At 2.5 V, coloring times are approximately equal to lightening times for the thinner devices. Slight differences are observed for the thicker devices of 180- and 230-μm thicknesses. Bleaching time is stabilized at 15 s for the thicker devices but is faster at 230 micrometers.

4.2. Electrochemical Measurements From ChrA and ChrC Experiments

Fig. 8 (left) shows a portion of Fig. 3, just for the 230 μm thickness device. The current and charge measurements were obtained with ChrA and ChrC experiments when applying 2.5 (from 0 to 60 s) and 0 V (from 60 to 120 s). For 2.5 V applied, a peak of current is observed, which is stabilized to a constant value at the first 30 s. Then, a negative peak current appears when short-circuiting the device, resulting in a decrease of the charge from t = 60 to t = 90 s. This negative current is due to the reduction reaction, or the release of the electrons of the radical cation (colored state) to the dicationic (colorless state) of viologen forms. The decrement, divided by the effective area, is the effective charge density ΔQ_{redox} used in the reduction reaction [11]. Fig. 9 (right) shows a 3-D plot relating the applied potential levels, i.e., ΔQ_{redox} and $ChrT_{600\,nm}$ at t = 30 s for the colored state of the different thickness devices. Increasing over 2.25 V (2.00 for 230 μm) resulted into no appreciable coloration change in the devices. Only the projections of the plot are shown for the sake of better visualization.

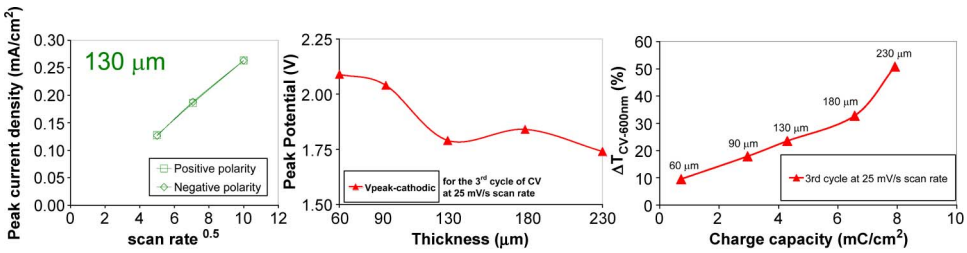

Fig. 9. (Left) Linear relationship between peak current densities and the square root of the scan rates for the 130 μm internal layer thickness device. (Middle) Thickness dependence cathodic peak potentials for positive polarity. (Right) Transmittance contrast (ΔT) at 600 nm versus charge capacity.

Coloration efficiency (CE) represents the ratio of the area of electrochrome, color of which is intensified by unit absorbance and the charge passed [12] and is calculated following expression (1):

$$\mathrm{CE} = \frac{\alpha d}{\mathrm{Q}} = \frac{\Delta A}{\mathrm{Q}} = \frac{\mathrm{OD}}{\mathrm{Q}} \tag{1}$$

where α is the linear absorption coefficient, d is the internal layer thickness, $\Delta \mathrm{A} = \mathrm{OD}$ is the absorbance contrast or optical density, and Q is the injected/ejected charge density at the coloring time. A maximum of 52 cm^2/C of CE at 600 nm is obtained for the 230-μm thickness device (with 39, 42, 40, and 49 cm^2/C of CE obtained for 180, 130, 90, and 60 μm internal layer thickness devices, respectively). A CE value of 136.6 cm^2/C was obtained on other thicker viologen EC devices manufactured following similar process [13].

4.3. Electrochemical Measurements From CV Experiments

From CV experiments, the peak of the current densities can be obtained [see Figs. 4 and 5 (left)]. It can be obtained that the redox reaction in the five devices is diffusion controlled, since the peak current density is proportional to the square root of the scan rate. As an example, Fig. 9 (left) shows the 130-μm device plot for both polarities of the voltage sweep. The third cycle of CV experiments at 25-mV/s scan rate [see Fig. 9 (middle)] shows a shift in the cathodic peak potentials Vpc from 1.74 to 2.09 V when decreasing the thickness of the device from 230 to 60 μm. The charge capacity of the CV experiments, calculated as the area containing each voltammogram divided by the scan rate, is related to the coloration observed in the devices. The transmittance contrast at 600 nm for CV experiments $(\Delta \mathrm{T}_{\mathrm{CV}-600\,\mathrm{nm}})$ is calculated from the simultaneous transmittance measurements [see Figs. 4 and 5 (left)]. Fig. 9 (right) shows that, for the devices characterized in this paper, the thicker the device, the higher the $\Delta \mathrm{T}_{\mathrm{CV}-600\,\mathrm{nm}}$, which is related to the charge capacity parameter. It is expected that devices thicker than 230 μm should show an increment of $\Delta \mathrm{T}_{\mathrm{CV}-600\,\mathrm{nm}}$ until a maximum value corresponding to an optimum thickness. Higher charge capacities over the optimum thickness value would result, in fact, into a decrement of $\Delta \mathrm{T}_{\mathrm{CV}-600\,\mathrm{nm}}$. $\Delta \mathrm{T}_{\mathrm{CV}-600\,\mathrm{nm}}$ for 230 μm breaks the linear dependence with the charge capacity, which indicates the closeness to the optimum thickness. Study on thicker devices will be carried out in future works for supporting this first approximation to the optimum internal layer thickness.

4.4. Electrochemical Measurements From EIS Experiments

Fig. 10 shows a 3-D Cole–Cole or Nyquist diagrams of the impedance dependence with thickness of the internal layer of the EC devices in colorless (up) and colored (down) optical states with 0- and 1.75-V dc bias applied, respectively. Linear scales up to 1 MΩ is used for visualizing the colorless state [see Fig. 10 (left)] and up to around 1 kΩ for the colored state [see Fig. 10 (right)]. Points at the lower frequencies fall at the high part of the plot for the colorless state and at the right part of the plots for the colored states. Nyquist diagrams of the devices at the colorless state with 0 V seems the one of a capacitor while at the colored state with 1.75 V shows a semicircle at high frequencies and a line at low frequencies. The diameter of the semicircle increases with the

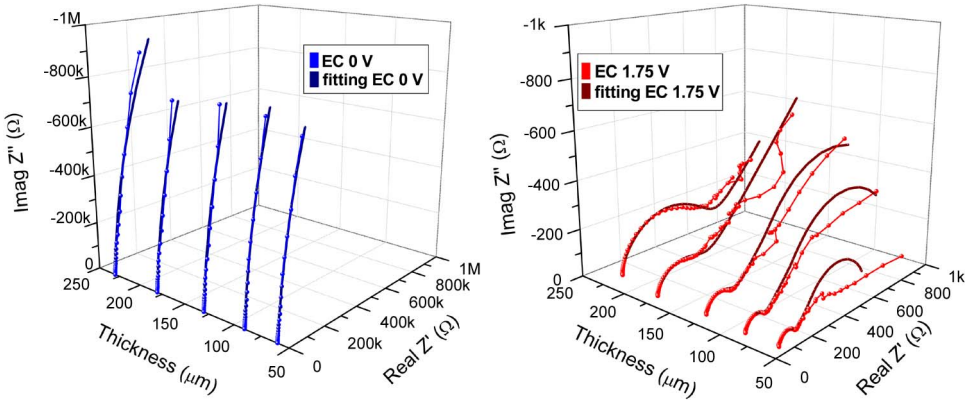

Fig. 10. Nyquist impedance thickness dependence: (left) at 0 V for colorless state, (right) at 1.75 V for colored state.

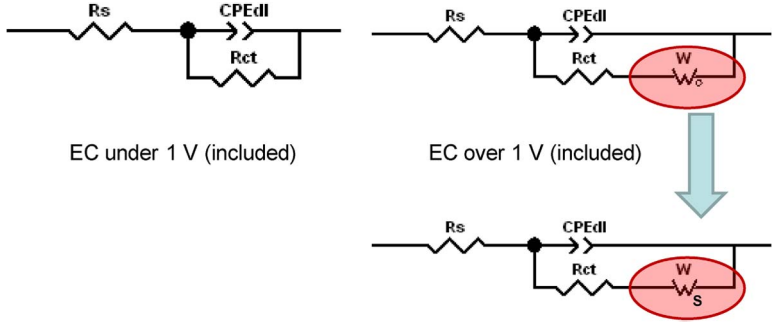

Fig. 11. EEC (equivalent electric circuit) model for EC devices under (left) and over (right) a threshold value of 1 V dc bias voltage. W_o must be replaced by W_s for thinner devices (right-down).

thickness. The imaginary part of the impedance Z″ goes to zero for thinner devices or continues increasing for thicker devices.

Impedance plots at 1.75 V were fitted to an EEC model shown in Fig. 11 [10]. This Randles EEC model has been proposed in other works with viologen [11], [14], [15] and also inorganic WO_3 (EC layer) and V_2O_5 (counter electrode) EC devices [16]. R_s is the electrical resistance of the electrodes and contacts. CPE is a constant phase element reproducing the double layer accumulation of charges near the working electrode [17]. CPE-P is an exponent showing the proximity of the CPE element to a capacitive behavior, i.e., as closer to 1, as closer to a capacitor. CPE-T is related to response time and capacity. R_{ct} is the resistance related with charge transfer. W_s and W_o are the short-circuit and open-circuit Warburg impedance elements, respectively, standing for the diffusion of charges at thinner and thicker devices, respectively. Nyquist diagrams of W_s and W_o at high frequencies match with the one of a CPE with phase angle of 45° and at low frequencies tends to infinite or to zero for W_o and W_s, respectively. W-R and W-T are resistive and temporal parts of the Warburg impedance, respectively. W_o was substituted by W_s for the thinner EC devices to fit the trend in Fig. 11(right), and thus, it can be concluded that the effective diffusion length of the charges is higher than thickness of the active layer of the EC device.

The fittings to this EEC model are plotted together with the measurements in Fig. 10, showing higher deviation at lower frequencies of the colored state, where the diffusion process takes place. Bode plots show a better fitting at low frequencies; logarithmic scale increases the error appearance at low frequencies: a χ^2 value under 0.02 was obtained for fittings, being under 0.01 at 60 μm thickness and higher at 230 μm. The fittings errors for the parameters were under 10% except for R_{ct} at low voltages and thicknesses (where R_{ct} is around MΩ) and for Warburg impedance

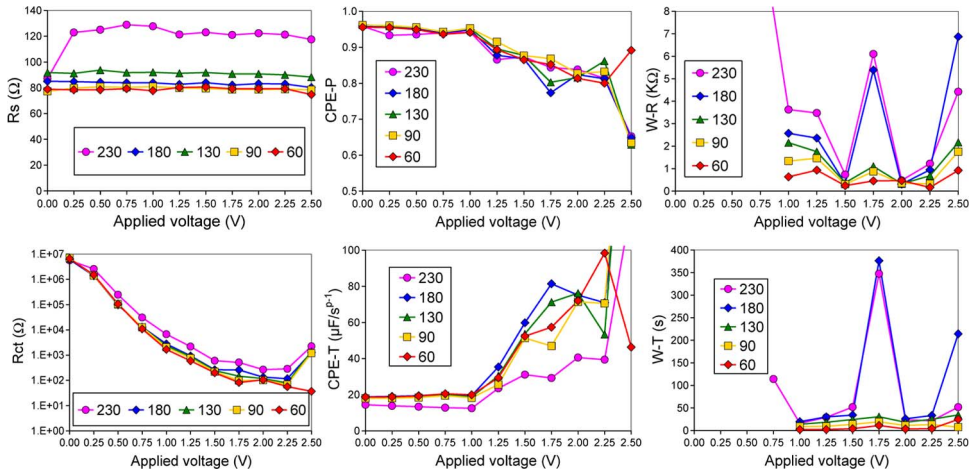

Fig. 12. Thickness and applied voltage dependence of the parameters of the EEC model.

parameters at higher thicknesses. W_o instead of W_s use for 180- and 230-μm thicknesses lead to a decrease of the fitting errors from over 200% to around 20%, improving χ^2 in an order of magnitude.

Fig. 12 shows the retrieved parameters and their dependence with voltage and thickness. Values of R_s around 80 Ω (120 Ω for 230 μm) are constant with voltage as expected. Values of R_{ct} have an exponential decay from 0 to 1.5 V, stabilizing at values between 100 and 700 Ω for the optically detected redox voltage (1.75 V), where anodic and cathodic potential peaks of CV experiments take place. W-R and W-T are jumping just at 1.75 V, but only for 180 and 230 μm thicknesses, when W_s is replaced by W_o. CPE-P shows a behavior close to a capacitor response only differing at colored states. CPE-T is constant at colorless states and increases at colored states to values between 20 and 100 $\mu F/s^p$. The electrical behavior of the colorless state from 0 to 1.25 V is the one of a CPE (being CPE-P $\approx$ 0.95) in series with R_s, which is mainly a capacitor, as it is observed in Fig. 10 (left), since the high R_{ct} value makes the parallel circuit to be neglected.

Relevant information about diffusion effects is derived from Fig. 13, which shows the Nyquist diagrams of the Warburg impedance elements simulated from the W-R and W-T parameters in Fig. 12, for the frequency range from 10 mHz to 1 MHz. For the five thicknesses studied, a high value of the Warburg impedance magnitude is observed at potentials of noncoloration in the devices (1.00 and 1.25 V), decreasing at 1.5 V, which corresponds to the threshold dc bias voltage in Fig. 2. The diffusion Warburg behavior follows with an increment, observed at 1.75 V, and a new decreasing at 2.00 V. This value is 2.25 V for the 60-μm case, which could be related to the shift on the peak potentials of CV experiments shown in Fig. 9 (middle); considering the 0.25 V steps of the experiment, it could have drifted to that value easily.

4.5. Relating Electrochemical Measurements From EIS and From ChrA and ChrC, and CV Experiments

Short-circuit W_s at low frequencies is half a semicircle in Nyquist plot, which matches with the one of a simple Randles cell (consisting on a R_s in series with a shunt of capacitor C_{dl} in parallel with R_{ct}). For the lowest frequency (close to a dc signal), the imaginary part W_s" tends to zero and the real part W_s' tends to the parameter W_s-R ($R_s + R_{ct}$ in a Randles cell). Hence, in Fig. 13, diffusion effect on 60-μm thickness device seems to be produced at 2.00 V rather than at the 1.75 V, which is the case for the other four devices, since their data exhibit only the high frequency behavior (45° slope). From CV experiments (see Figs. 4 and 5), the rate of the reaction seemed to be slower as the thickness increased. On the other hand, since, from ChrA experiments [see Fig. 8 (left)], a continuous electrical current was observed once coloration process stabilized, the fitting to the EEC model should be in all cases using W_s and not W_o, since W_o'' at low frequencies tends to infinite (i.e.,

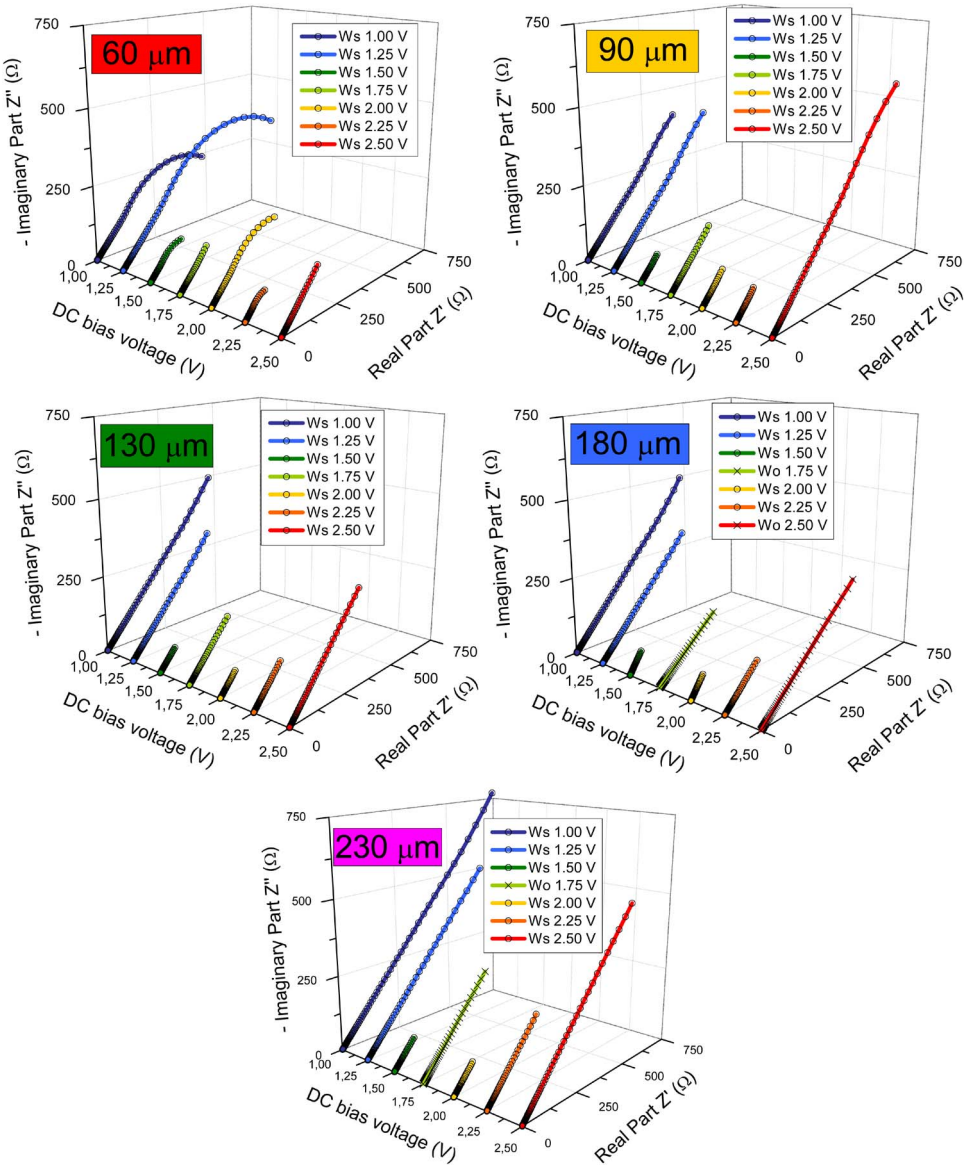

Fig. 13. Nyquist diagram of the Warburg impedance element for different potentials and thicknesses.

an open circuit) and no electrical current consumption should be observed. Thus, for a perfect fitting, perhaps new components should be added to the proposed EEC model, in order to simulate the effects of the second redox reaction observed in viologen forms, from radical cation (colored state) to neutral species (undesired state for switching).

Fig. 14 (left) shows the variation of the magnitude of the Warburg impedance $|Z_W|$ observed in Fig. 13, at the lowest frequency of 10 mHz, with the different dc bias voltage levels, for the five different thicknesses. The jump observed in EIS experiments at 1.75 V (2.00 V for 60 μm) is related to the cathodic potential peaks Vpc observed in CV experiments at 25-mV/s scan rate in Fig. 4 (left). Fig. 14 (right) shows the voltammograms of the third cycle of the positive sweeps for CV experiments for the different thicknesses. New measurements at dc bias voltage levels between 1.75 and 2.25 V with 0.05-V steps, or even lower (instead of 0.25 V), could derive to a better concordance of both EIS and CV experiments in order to obtain a relation between the redox reaction cathodic potential peaks Vpc and the diffusion process.

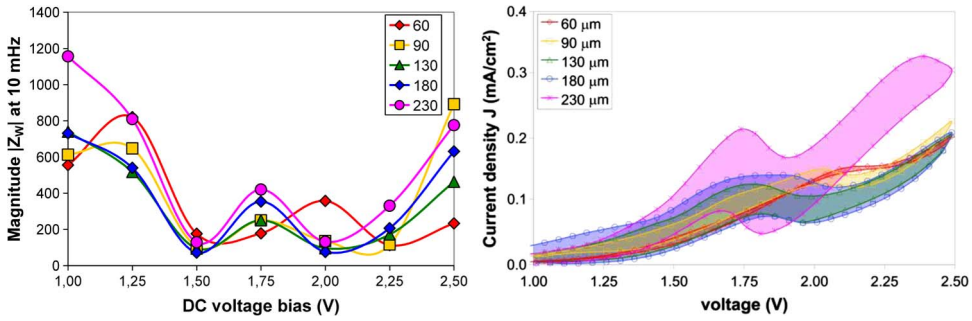

Fig. 14. (Left) Warburg impedance magnitude at 10 mHz. (Right) Voltammograms from the 3rd cycle of CV experiments at 25 mV/s scan rate.

5. Conclusion

The increment of the optical transmittance contrast, between colorless and colored states of viologen-based EC devices, has been achieved by increasing the thickness of their internal layer, which results into the increments of the effective charge density and the charge capacity. The parameters of the EEC model depend on the thickness and on the dc bias voltage levels, being directly related to the coloration states. The increment of the diffusion length has been determined for thicker devices by the behavior of the fitted Warburg impedance. The peak of current observed with CV experiment has been determined to match with the higher diffusion impedance values fitted by the EIS experiment. The thicker the EC device, the slower the diffusion process.

References

[1] P. M. S. Monk, *The Viologens: Physicochemical Properties, Synthesis and Applications of the Salts of 4,4%-Bipyridine*. New York: Wiley, 1998.
[2] E. M. Kosower and J. L. Cotter, "Stable free radicals. II. The reduction of 1-methyl-4-cyanopyridinium Ion to methylviologen cation radical," *J. Amer. Chem. Soc.*, vol. 86, no. 24, pp. 5524–5527, Dec. 1964.
[3] A. G. Evans, N. K. Dodson, and N. H. Rees, "Study of bipyridyl radical cations. Part III. Reaction of paraquat radical cation with oxygen and with chromic ions in methanol," *J. Chem. Soc., Perkin Trans.*, vol. 2, no. 7, pp. 859–863, 1976.
[4] Electrochromic layer and devices comprising same, EP1443092 A3, Mar.15, 2006.
[5] N. J. Goddard, A. C. Jackson, and M. G. Thomas, "Spectrelectrochemical studies of some viologens used in electrochromic display applications," *J. Electroanal. Chem. Interfacial Electrochem.*, vol. 159, no. 2, pp. 325–335, Dec. 1983.
[6] R. J. Mortimer and J. R. Reynolds, "An *in situ* colorimetric measurement study of electrochromism in the di-n-heptyl viologen system," *Displays*, vol. 29, no. 5, pp. 424–431, Dec. 2008.
[7] G. Bar, N. Larina, L. Grinis, V. Lokshin, R. Gvishi, I. Kiryuschev, A. Zaban, and V. Khodorkovsky, "RGB organic electrochromic cells," *Sol. Energ Mat. Sol. Cells*, vol. 99, pp. 123–128, Apr. 2012.
[8] C. Pozo-Gonzalo, J. Pomposo, H. Grande, M. Salsamendi, and R. Marcilla, "Composiciones electrocrómicas basadas en viológenos, formulables y aplicables a temperatura ambiente," Patent P200 800 258, May 31, 2010.
[9] J. Bruinink, C. G. A. Kregting, and J. J. Ponjeé, "Modified viologens with improved electrochemical properties for display applications," *J. Electrochem. Soc.*, vol. 124, no. 12, pp. 1854–1858, 1977.
[10] D. Barrios, R. Vergaz, J. C. Torres, J.-M. Sánchez-Pena, A. Viñuales, and M. Salsamendi, "Electrochromic materials and devices," in *Proc. Mater. Res. Soc. Symp.*, San Francisco, CA, Apr. 26/27, 2011, vol. 1328E.
[11] R. Vergaz, D. Barrios, J.-M. Sanchez-Pena, C. Pozo-Gonzalo, and M. Salsamendi, "Relating cyclic voltammetry and impedance analysis in a viologen electrochromic device," *Sol. Energy Mater. Sol. Cells*, vol. 93, no. 12, pp. 2125–2132, Dec. 2009.
[12] P. M. S. Monk, *Handbook of Advanced Electronic and Photonic Materials and Devices, vol. 7, Liquid Crystals, Displays and Laser Materials, Electrochromism and Electrochromic Materials for Displays*. New York: Academic, 2000.
[13] C. Pozo-Gonzalo, M. Salsamendi, A. Viñuales, J. A. Pomposo, and H.-J. Grande, "Highly transparent electrochromic plastic device that changes to purple and to blue by increasing the potential," *Sol. Energy Mater. Sol. Cells*, vol. 93, no. 12, pp. 2093–2097, Dec. 2009.
[14] R. Vergaz, D. Barrios, J. M. Sanchez-Pena, C. Pozo-Gonzalo, M. Salsamendi, and J. Pomposo, "Impedance analysis and equivalent circuit of an all-plastic viologen based electrochromic device," *Displays*, vol. 29, no. 4, pp. 401–407, Oct. 2008.
[15] M. Marescaux, F. Beunis, F. Strubbe, and K. Neyts, "Electrochromic materials for electronic paper," in *8th FIRW PHD Symp.*, Ghent, Belgium, 2007.
[16] P. Baudry and M. A. Aegerter, "Electrochromic window with lithium conductive polymer electrolyte," *J. Electrochem. Soc.*, vol. 138, no. 2, pp. 460–465, Feb. 1991.
[17] E. Barsoukov and J. R. Macdonald, *Impedance Spectroscopy: Theory, Experiment, and Applications*. New York: Wiley, 2005.